2023 IEEE International Conference on Robotics and Automation (ICRA 2023)
May 29 - June 2, 2023. London, UK

Development and Evaluation of a Robotic Vessel Positioning System for Semi-Automatic Microvascular Anastomosis

Jesse Haworth
Laboratory for Computational Sensing and Robotics
Johns Hopkins University
Baltimore, MD, United States
jhawort2@jhu.edu

Justin Opfermann, MS
Laboratory for Computational Sensing and Robotics
Johns Hopkins University
Baltimore, MD, United States
jopferm1@jhu.edu

Michael Kam, MS
Laboratory for Computational Sensing and Robotics
Johns Hopkins University
Baltimore, MD, United States
mkam2@jhu.edu

Yaning Wang
Department of Electrical and Computer Engineering
Johns Hopkins University
Baltimore, MD, United States
ywang511@jhu.edu

Robin Yang, D.D.S., M.D.
Department of Plastic and Reconstructive Surgery
Johns Hopkins Medicine
Baltimore, MD, United States
ryang14@jhmi.edu

Jin U. Kang, PhD
Department of Electrical and Computer Engineering
Johns Hopkins University
Baltimore, MD, United States
jkang@jhu.edu

Axel Krieger, PhD
Laboratory for Computational Sensing and Robotics
Johns Hopkins University
Baltimore, MD, United States
axel@jhu.edu

***Abstract*—This paper describes a novel tissue positioning system with an integrated suturing robot and demonstrates its ability to perform semi-automatic anastomoses of synthetic blood vessels. We began with a finite element analysis-based design consideration for achieving adequate grasping of blood vessels to demonstrate robust performance under expected clinical forces. We then conducted standardized positioning tests to measure the repeatability of the system and incorporated a high-resolution optical coherence tomography (OCT) fiber imaging sensor within the tip of the suturing tool to provide position feedback of the robot during a suturing task. Using the microvascular positioner and OCT sensor, the system performed semi-automatic suturing of synthetic 5 mm diameter blood vessels (N=4), and the suture quality was evaluated for consistency in spacing, bite depth, percent lumen reduction, and maximum suture strength. The system completed the task in an average time of 31.75 minutes. The samples had zero missed stitches, average spacing of 1.64 mm, an average bite depth of 2.14 mm, an average lumen reduction of 57.98%, and an average suture strength of 3.13 N.**

Keywords—Semi-Automatic, robotic suturing, microvascular anastomosis, OCT imaging, microsurgery

I. INTRODUCTION

Anastomosis is a surgical reconstructive technique that involves the joining of two luminal structures. Vascular anastomosis (joining two blood vessels) can be particularly challenging as small vessel diameters must be joined to form a leak-free connection that can withstand intraluminal blood pressures [1]. In 1902 Alexis Carrel pioneered the field of vascular surgery by developing the first surgical technique to join two vessels. In his technique, Carrel triangulated the two vessels by equally placing three staging sutures around the vessel wall which were used to reapproximate and align the vessels so a continuous running stitch could be applied [2]. This technique was later refined to include placing sutures using a patch technique whereby the lumen was opened so sutures could be easily placed along the tissue edge [3].

Despite recent advancements in surgical imaging, tools, and techniques that enable reconstructive microsurgery in vessels smaller than 1 mm in diameter [4], [5], microvascular anastomosis remains a challenge [6]. Despite microvascular surgery being perform in the open setting under a microscope, inadequate visualization can lead to suturing of both walls of the vessel, while non-absorbable suture [7] and anastomotic leak are responsible for significant complications such as early dehiscence (rupture) or late stricture which occur in up to 25-30% of visceral transplantation anastomoses [8]. For even the most skilled

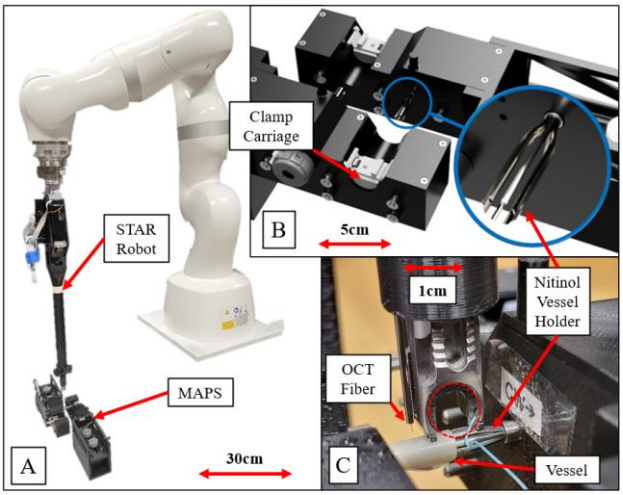

Fig. 1. A: Smart tissue autonomous robot (STAR) positioned over microvascular positioning system (MAPS). B: MAPS clamp carriage and nitinol vessel holder. C: STAR in suturing positing with OCT imaging fiber. Circular needle path shown with red dashed line.

*Research reported in this paper was supported by the National Institute of Biomedical Imaging and Bioengineering of the National Institutes of Health (NIH) under award 1R01EY032127 and the National Science Foundation (NSF) Foundational Research in Robotics under CAREER award 2144348. The content is solely the responsibility of the authors and does not necessarily represent the official views of the NIH or NSF.

979-8-3503-2365-8/23/$31.00 ©2023 IEEE

surgeons, anastomotic thrombosis occurs in 0.5–10%. These complications significantly undermine the clinical outcomes, and diminish the quality of life for affected patients, and can make repeat surgery extremely difficult [9]. Additionally, a single microvascular anastomosis may take more than 40 minutes to complete [10] which puts stress on time sensitive surgeries such as limb or organ transplantation.

Advances in medical robotics have enabled highly dexterous and precise surgical systems that reduce surgical time and improve patient recovery [11]. Tele-operated robots such as the da Vinci Surgical System (Intuitive Surgical, Sunnyvale, California) [12] are already used in urology, gynecology, cardiothoracic, and general surgery, but have had more limited success in microvascular anastomosis [13] as functional outcomes depend on the proficiency and skill of the surgeon which varies greatly between individuals. The Smart Tissue Autonomous Robot (STAR) has outperformed expert surgeons in suture quality and consistency in preclinical open [14] and laparoscopic [15] studies. However, at present the imaging system and suturing tools are too large to perform anastomosis on microvasculature.

In this paper we overcome this limitation by introducing a novel microvascular anastomosis positioning system (MAPS) that can be integrated with STAR to enable semi-automatic anastomoses of vessels 5 mm in diameter. MAPS is a specialized robotic tool for manipulating blood vessels which enables vessel suturing with the STAR robot. As a first contribution we describe the design and development of MAPS, capable of grasping and positioning synthetic blood vessels as shown in Fig. 1. Performance of the positing system is reported including finite element analysis and repeatability of positioning. Second, we integrated the MAPS with STAR to create a microvascular suturing system. Optical coherence tomography (OCT) fiber image sensor was used for positioning feedback between the MAPS and STAR system so that the needle trajectory is aligned correctly with the blood vessel. Finally, the overall system was evaluated by performing semi-automatic vessel anastomosis in synthetic vascular grafts (N=4). The quality of the suture line was evaluated for consistency in suture spacing, suture bite depth, percent luminal reduction, and mean tensile strength which was shown to be within clinical requirements.

II. Prior Works

A. Manual Anastomosis Tools

While the conventional method for manually performing microvascular anastomosis is still performed with a standard suturing toolkit, several manual tools have been created to make performing anastomosis easier. The Cardica C-Port system streamlines the creation of an end-to-side anastomosis in vessels as small as 1mm inner diameter by utilizing small staples to create the joint [16]. The device is not indicated for end-to-end anastomosis and in most cases traditional manual sutures are needed to finish the hemostatic seal. Another commonly used device is the venous coupler. This is an implant comprised of two barbed halves which join two vessels together. Using the device is simple and reduces the total amount of time it takes to perform an end-to-end anastomosis [17], however a retrospective study found that anastomoses formed with the coupler had a higher revision rate and higher occurrence of thromboses than anastomoses performed with sutures [18]. Additionally, these methods have presented complications when used in arterial anastomosis [19]–[22]. Therefore, hand sutured techniques remain the gold standard for vessel anastomosis [4].

B. Teleoperated Robotic Anastomosis

Advances in imaging and robotics technology make robotic microvascular anastomosis a promising alternative to sutureless devices. The da Vinci Surgical System by Intuitive is one such robot that uses a teleoperation control strategy to mirror a surgeon's hand motions with highly dexterous laparoscopic tools. The system also provides motion scaling to remove surgical tremors which are magnified in microvascular suturing [23]. The system has been trialed in microvascular applications [24] but widespread use has been limited because the tools sets are designed for general surgery and the vision system does not have fine enough resolution at magnification for microsurgical applications [25]. Alternatively, Cau describes the design and evaluation of the MicroSure Robot (MicroSure, Eindhoven, The Netherlands), a light weight teleoperated robot designed specifically for microvascular anastomosis [26]. MicroSure incorporates a surgical microscope to solve the magnification and resolution limitations of the da Vinci system and has a surgical tool set designed specifically for microsurgery [27]. Similarly, Mitsuishi et. al describe a teleoperated microsurgical robot [28] which can anastomose synthetic vessels 0.3 mm in diameter. However, despite the improved dexterity and reduced tremor, both tele-operated systems suffer from increased procedure times compared to manual operation.

C. Autonomous Robotic Anastomosis

Autonomous surgical robotic systems take advantage of the accuracy and repeatability of robotics to complete repetitive sub-tasks of a surgical procedure such as needle positioning [29] and suture path planning [30]. As Sen et al demonstrated in 2016, it was possible to perform autonomous multi-throw, multilateral suturing of synthetic tissues using a da Vinci Research Kit (DVRK) if a sequential convex programming strategy was used [31]. More recently, Saeidi et al, demonstrated that autonomous laparoscopic anastomosis was feasible in a preclinical model using the STAR system [15], and that the anastomosis was more consistent than samples sutured by expert surgeons using manual or tele-operated techniques. The autonomous suturing was performed

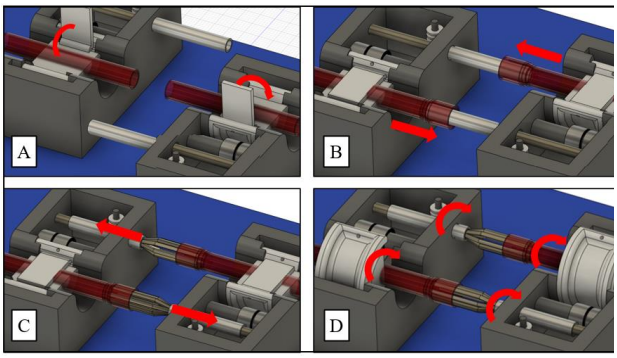

Fig. 2. MAPS System workflow. A: Vessels loaded into clamps. B: Vessels loaded over sheaths. C: Sheath is pulled back allowing the nitinol to expand inside the vessels. D: Clamp carriage and nitinol rotated to move vessels between suturing positions.

in small intestines and was enabled by a novel structured light laparoscope and laparoscopic suturing tool. However, while the performance was adequate for small intestine, the resolution of the camera and deformation of the anastomosis exceeds the size of microsurgical vasculature. Thus, as a first step towards automating microvascular anastomosis, we proposed that developing MAPS and integrating an OCT fiber imaging sensor, would enable accurate and repeatable anastomosis in 5 mm diameter blood vessels with STAR. This system simplifies tissue manipulation, has the potential to automate vascular and microvascular anastomoses, and could lead to improved outcomes.

III. Materials and Methods

A. MAPS Design

During standard microvascular anastomosis procedures, as performed in many transplant procedures, it is common for the surgeon to use a double approximator clamp to hold the vessels while suturing in an open surgical setting under an operating microscope. The clamps on either side of the approximator are used to prevent blood from flowing into the vessel while suturing is done in between them. Once the sutures on the front half of the vessel are complete, the approximator clamp is flipped over 180 degrees, rotating the vessels and allowing the surgeon to suture on the back half [5]. Our robot design attempts to emulate this style of workflow by rotating the vessels to access suture positions. Because the procedure is performed in an open setting, MAPS form factor could be larger, with physician interviews confirming it was appropriate for the surgical scene.

A demonstration of the MAPS workflow is shown in Fig 2. First, the vessels were loaded into the clamps on either side as in Fig. 2A. Next, each vessel was loaded over the sheathed nitinol (Fig. 2B), which was feasible as physicians currently load over vessel dilating forceps. Once the nitinol was unsheathed, the tines expanded, which gripped the vessel and fixed its orientation (Fig. 2C). The system was designed to rotate the nitinol holders and clamped vessel in tandem as in Fig. 2D.

Each half of the system was driven using two stepper motors. The first motor, the sheathing motor, rotated a pulley attached to its shaft, see Fig. 3A. Rotating the pulley actuated either the left or right cable. Each cable was attached to the sheath and wrapped around a pulley on either end of the travel. Then, when the stepper motor was moved, the nitinol was sheathed or unsheathed. A limit switch on either end of the sheath's travel informed the system when to stop. The second stepper motor drove the rotation of the nitinol and clamp carriage together, which was also referred to as the stage. The motor rotated a pulley which was attached to two pull wires, see Fig. 3B. These pull wires were coupled to a corresponding pulley in the device. When the stepper motor was actuated, the pulley in the device was rotated. The pulley was attached to a shaft along with a 25-tooth gear. This gear drove a larger 56 tooth gear, also called the large gear, which was fixed to the nitinol vessel holder. A US Digital E4T encoder was mounted to the nitinol on the outside of the housing which allowed the system to track orientation.

To ensure the clamp rotated in unison with the nitinol, the clamp was attached to a carriage that had a circular slot which

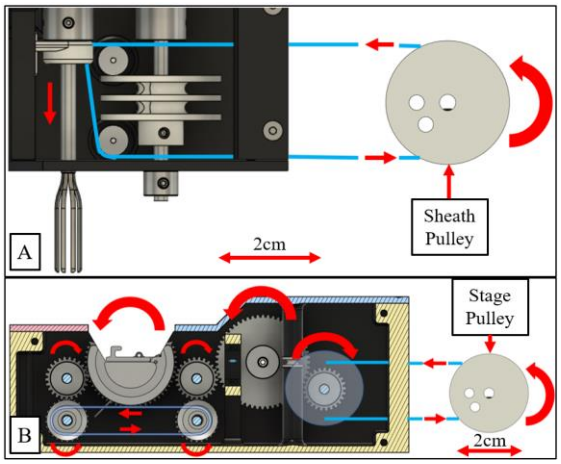

Fig. 3. A: Top view of the MAPS illustrating motion during sheath actuation. B: Front view of MAPS showing motion during stage rotation.

allowed it to rotate in the device housing. On the outside of the carriage was a geared edge with 56 teeth to match the large gear, but to ensure the top of the clamp was accessible, the teeth did not cover the full circumference. Because of this the carriage had only 37 teeth but maintained the same spacing and pitch diameter as the large gear. The large gear rotated a smaller 25-tooth gear which drove the clamp carriage. To ensure the carriage continued to be driven when the 25-tooth gear was not engaged with the teeth of the carriage, another gear on the opposite side of the carriage also drove the carriage. This gear was rotated by a belt and a small series of gears under the carriage, which synchronized the left 25-tooth gear with the right 25 tooth gear.

MAPS was designed using Fusion 360 (Fig. 1B). Smaller plastic components such as the clamp carriage and pulleys were 3D printed using an Anycubic Photon SLA printer and photopolymer resin. Larger components such as the housing were printed with PLA on a Creality CR-10 V2 FDM printer.

Each half of the system was controlled by an Arduino Mega 2560 which controlled two TMC 2130 stepper motor drivers. The limit switch and encoder were connected to the Arduino and the system was controlled by breadboard buttons. There were 5 buttons for controlling each half of the system, these buttons included: sheath toggle, rotate clockwise 45°, rotate counterclockwise 45°, rotate clockwise 1°, and rotate counterclockwise 1°. One 45° rotation moved the system from one suture position to the next, while the 1° rotation was used to fine tune the position.

B. Nitinol Vessel Holder

The centerpiece of the MAPS design was the nitinol vessel holder shown in Fig. 1 and Fig. 4. This component allowed the system to hold the vessel open from the inside, providing counterforce for the needle to pass through the tissue without puncturing the opposite wall of the vessel. The component was made from a laser-cut nitinol tube which had been heat set to an expanded position. Gaps between each of the nitinol tines allowed space for the needle and helped to ensure the consistency of suture spacing. There were 8 gaps in the nitinol for 8 sutures to be placed, which was decided based on similar microvessel surgeries [32] and physician interviews. Because of the superelastic properties of the nitinol, the holder could be sheathed into a much smaller diameter, allowing for easy

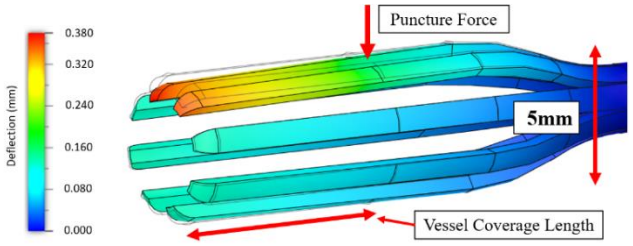

Fig. 4. FEA of nitinol vessel holder. Red areas mean maximum deflection, while blue means no deflection. (Fusion 360)

vessel loading over the nitinol. Once unsheathed, the nitinol expanded inside the vessel, holding it from the inside.

To ensure the nitinol component would meet the clinical needs of the suturing procedure, radial force and puncture force measurements were taken from the synthetic blood vessels (Microvessel, 3-Dmed, Franklin, OH) that were also used for feasibility testing. 3-Dmed synthetic tissues offer similar suturing and elasticity properties to real tissue. These results were used to define finite element analysis (FEA) loads in simulation which enabled the design of the nitinol to be optimized to have the smallest possible outer diameter (OD) while still adequately supporting the vessel during suturing. Other design constraints were availability of stock nitinol components, laser cut width, manufacturability, and the force required to sheath the nitinol. Resulting collapsed nitinol is 50% the diameter of the vessel which enabled easy insertion into the vessel.

The puncture force was tested with the vessel stretched to a range of diameters, but no relationship was found between expansion and force. For our analysis we used the maximum recorded force value of 0.31 N and added a 20% safety buffer. Hence, the force used for analysis was 0.37 N.

The vessel was pressurized with saline, and the correlated OD was measured throughout using ImageJ (National Institutes of Health, Bethesda, MD) [33]. The pressure results were used to calculate a linear regression which enabled estimation of radial pressure on the nitinol holder when the tissue was expanded to a given diameter. The resulting linear equation (1) had an R^2 value of 0.93. Vessel OD was measured in mm and pressure was in kPa.

$$Vessel\ OD = 0.0715 * Pressure + 4.9275 \quad (1)$$

During optimization in FEA an expanded OD of 5.5 mm was selected to minimize OD and deflection. By plugging 5.5 mm into the linear regression and adding a 20% buffer, this produced an anticipated radial pressure of 9.61 kPa.

Using the calculated radial pressure and maximum puncture force, the loads in the model were defined for FEA. Fusion 360 with the ADS NASTRAN solver was used for the simulation. The radial pressure was applied to the OD of the nitinol tines where the vessel would be loaded, and the puncture force was applied to the approximate suture site (8.5 mm along the length of the tines). Results are shown in Fig. 4. The maximum deflection was 0.38 mm and the deflection at the puncture force location was 0.20 mm. This deflection was anticipated to be acceptable for performing the suture. Additional nitinol holders would need to be manufactured for use in other vessel sizes.

C. STAR Integration

Suturing was performed using the STAR system which has been described in detail in earlier works [14], [15]. The STAR was outfitted with a circular needle drive based on the Endo360 suturing tool (EndoEvolution, North Chelmsford, Massachusetts) and was compatible with 2-0 and 3-0 polyester suture. In this study, the control workflow used a high-level task planner so that an operator could control STAR in a semi-automatic mode. The workflow combined a sequence of robot motions that traverse pre-planned points as well as stitch placement routine. A total of 8 points could be taught prior to the procedure and were preloaded to the task planner. The operator then specified the point sequence of execution in the high-level task planner and defined the automatic sections of the robot motion. When executing the routine, the system would pause the task planner prior to suturing so that alignment of the suturing tool and target tissue may be verified with the integrated OCT imaging. Once the operator confirmed the position of the suturing tool, the system applied a suture, and the task planner resumes automatic motion along the pre-planned points. For low-level motion planning of STAR, Moveit! was utilized with integrated Pilz motion planner to interpolate point-to-point and linear motion with smooth trajectories. The Cartesian trajectory was transformed to waypoints in joint space via inverse kinematics. OROCOS real-time toolkit was used for real-time control of STAR components including the robot system and the suturing device.

D. OCT Imaging

The system used common-path optical coherence tomography (OCT) to provide real-time positioning feedback of the suturing tool with respect to the vessel and nitinol tines. The signal was acquired using a single-mode fiber (1060XP, Core Index: 1.45, Thorlabs, Newton, NJ, USA) that was connected to a swept-source OEM engine (AXSUN, Billerica, MA, USA), a broadband mini optical attenuator (BVOA-1050-L-10-FA, OF-Link, ShenZhen, China), a broadband circulator (OF-Link, BPICIR-1060-H6, ShenZhen, China), a Camera-Link frame grabber (PCIe-1433, National Instrument, Austin, TX, USA) and a laptop (Precision 5520, DELL, Round Rock, TX, USA). The interference signal came from the sample and the interface between fiber and outside medium. The original spectrum data was sampled by a frame grabber (National Instrument, PCI-E-1433) and processed parallelly with a discrete graphics card on the laptop to achieve the sensing speed of 100 Khz. By combining the sample and reference beam with the same single-mode fiber, the system was immune to dispersion and polarization noise. The OCT fiber imaging sensor was integrated into the suturing tool by gluing the

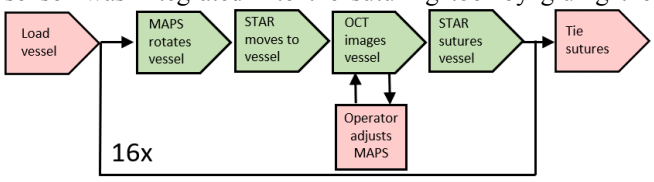

Fig. 5. Workflow for semi-automatic placement of one suture. Routine repeats sixteen times for one anastomosis. Red: Manual. Green: Automatic.

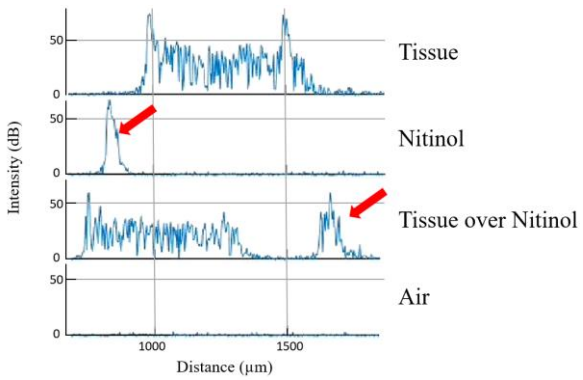

Fig. 6. OCT imaging data as it was displayed during the procedure. Spikes associated with nitinol are noted with red arrows.

single mode fiber within a stainless-steel hypotube that was embedded within a distal sleeve as shown in Fig. 1C. The sleeve was oriented such that the fiber was co-planar with the path of the suturing needle and aligned the OCT signal with the target tissue. The center wavelength was 1060 nm with an output power of 2 mW which provided an axial resolution of 4.5 µm with a scanning depth of 3.7 mm in air.

E. Semi-Automatic Suture Placement Workflow

The workflow to perform semi-automatic suture placement with the described system is detailed in Fig. 5. We note manual tasks are in red, and tasks performed semi-automatically in green. The workflow described is for a single suture throw and must be repeated a total of sixteen times for the complete anastomosis. The procedure began with STAR at a home position while the operator manually loaded two vessels onto the MAPS platform. Next, STAR automatically moved the suturing tool to the first suture location on the left vessel. When at the suturing position, the operator observed the OCT imager and determined if MAPS should be used to perform positioning adjustments to the orientation of the blood vessel. MAPS could be used to apply fine rotational adjustments of 1° to correct any errors in positioning. After confirming the needle location, the robot applied the first throw, then automatically moved to the right vessel, and waited for manual confirmation to apply the second throw. After both suture throws had been completed, STAR automatically moved back to the home position while the operator used MAPS to rotate the vessels 45°. The suture routine was then repeated, and knots were tied manually after all sutures had been thrown.

IV. Experiments and Results

A. Repeatability of Stage Rotation

To test the repeatability of the system, the MAPS rotation stage was rotated in 45° increments through the full motion of the robot. This includes starting at the zero position, rotating 180° in one direction, 360° in the opposite direction, and then back 180° to the starting point. This resulted in 16 steps for the full motion. ImageJ was used to record the angle between each increment. For the left stage the average was 44.51° and a standard deviation of 2.08°. For the right stage the average was 49.31° with a standard deviation of 9.68°.

B. OCT Imaging Feedback

During the anastomosis procedure, the operator was able to determine if the OCT, which was aligned with the plane of the needle, was above just air, tissue, nitinol, or both tissue and nitinol. An example of the OCT output is show in Fig. 6 with the nitinol signal identified by an arrow.

C. Suture Testing with STAR System

To setup the entire system, MAPS was fixed onto a table in the field of the STAR system, see Fig. 1A. A test vessel was loaded into the system which was used for reference to teach the STAR robot all the points in the workflow. The OCT display was setup in view of the operator to allow the operator to use the feedback from the OCT to adjust the spacing of the sutures before passing the needle. Every 4 sutures, as the suture was depleted, the needle and suture were replaced.

For evaluating the setup, four anastomoses were performed on synthetic vessel samples from 3D-Med, placing 8 sutures in each vessel. Any necessary adjustments to the spacing based on OCT feedback were recorded. For the right stage of MAPS, the average angulation adjustment per stitch was 0.97°. For the left stage the average angulation adjustment per stitch was 0.16°.

Beginning and end times of all trials were recorded. Procedure duration ranged from 27 to 35 minutes with an average of 32 minutes. Anastomosis duration was faster compared to clinical anastomoses ranging from 40 to 75 minutes [10], however our trials did not include time to tie off sutures. Additionally, a few issues were noted during the procedure. A communication error with STAR resulted in a 21-minute pause during trial 4 which was subtracted from the total time. During sheathing at the end of each procedure the nitinol tended to catch the suture thread, requiring an additional sheath cycle to remove the tissue. The system successfully placed 64 consecutive sutures without missing the vessel tissue, crossing, or tangling suture threads. Human assistance was only needed on 12 sutures to adjust the spacing via OCT feedback. No sutures missed the vessel or punctured both walls. Additionally, no stretching, tearing, or other trauma was observed from MAPS handling the tissue.

D. Suture Spacing and Bite Depth

Pictures of sutured vessels were taken, and measurements of suture spacing and bite depth were recorded using ImageJ. Examples of the sutured vessel are shown in Fig. 7 where suture spacing is defined as the distance between two consecutive sutures, and bite depth is the shortest distance from the point of a suture on the vessel wall to the cut edge.

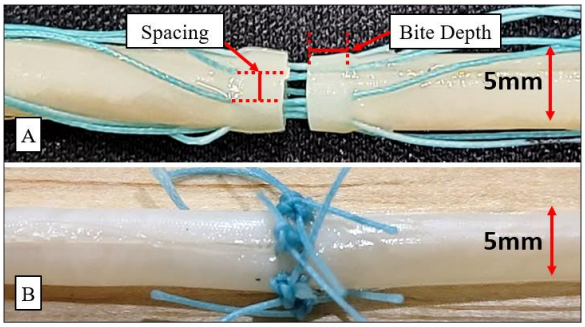

Fig. 7. A: Sutured vessel spacing and bite depth measurements. B: Sutured vessel after sutures have been tied off.

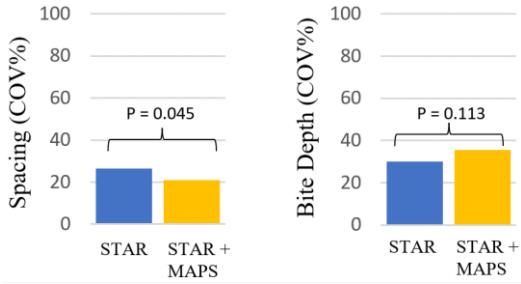

Fig.8. COV comparison between STAR system alone and STAR combined with MAPS.

For spacing and bite depth the averages were 1.64 mm and 2.14 mm, respectively. Standard deviations were 0.34 mm and 0.76 mm. Ideal suture spacing for the tissue was 1.77 mm.

To compare the vascular suturing performance to past anastomoses with STAR, we normalized the data by dividing the average suture spacing and average bite depth by their respective standard deviations to obtain the coefficient of variance for each metric (COV). The COV for microvasculature suturing was calculated to be 20.9% for spacing and 35.6% for bite depth. Prior studies using the STAR without using MAPS had achieved a COV of 26.36% for spacing and 29.99% for bite depth [15]. Using Forkman's method described in [34] and a statistical significance level of 0.05, we found that STAR had more consistent suture spacing with the MAPS system ($p = 0.045$), while no significant difference in bite depth was observed ($p = 0.113$) (see Fig. 8).

E. Lumen Reduction

After spacing and bite depth measurements were taken, the sutures were manually tied off using a surgeon's knot. Pictures were taken of the cross-section of each anastomosis and one non-sutured vessel sample. ImageJ was then used to calculate the percent reduction in area (TABLE I).

TABLE I. LUMEN REDUCTION MEASUREMENTS

Lumen Reduction							
Sample:	***Norm***	***1***	***2***	***3***	***4***	***Mean***	***SD***
Lumen Area (mm^2)	8.87	3.42	4.38	4.38	2.72	3.72	0.81
Percent Reduction (%)	N/A	61.4	50.5	50.5	36.3	57.9	9.15

F. Pull Force

Each of the anastomosis samples were tensioned in a tensile tester at a strain rate of 1 mm/second along with one intact synthetic vessel sample and one hand-sutured sample. The peak forces are recorded in TABLE II.

TABLE II. PULL FORCE TESTING SUMMARY

Pull Force							
Trial:	***Vessel***	***1***	***2***	***3***	***4***	***Mean***	***SD***
Peak Force (N)	6.77	2.88	3.18	3.56	2.88	3.13	0.32

Other studies have measured the tensile strength of a hand-sutured anastomosis to be 3.64 N with a standard deviation of 2.2 N when using porcine coronary arteries [35]. All the pull force results in this paper were well within one standard deviation of porcine artery data. Therefore, anastomoses from MAPS produce sufficient tensile strength.

V. DISCUSSION AND CONCLUSION

MAPS successfully performed 4 anastomoses when paired with the STAR Robot and OCT fiber imaging sensor. When compared to previous STAR studies the MAPS system reduced variance in suture spacing, but not in bite depth. This was due to bite depth placement being driven by pre-programmed points and not adapting to the tissue placement. OCT was shown to differentiate between air, tissue, nitinol, and tissue over nitinol. Integrating OCT into the control loop allowed MAPS and STAR to automatically position the suture relative to the tissue. Additional issues in variance were caused by encoder miscounts in the MAPS stage, and tissue movement on the nitinol holder. Changes to encoder mounting would improve repeatability and modifying the outer surface of the nitinol with etching or coatings that are used in other cardiovascular devices would improve vessel grip.

Leak testing is an important step in demonstrating the efficacy of this system. Such a test was not able to be performed on the phantom 3-Dmed tissue samples. Air leaked through the needle insertion site of these synthetic blood vessels, which made a pressurized test of the anastomosis unfeasible. Future testing will need to be done on ex-vivo tissue to enable leak testing. In place of this test, the pull force test was performed and sufficient tensile strength was shown.

Additionally, we considered the percent lumen reduction as a marker for clinical success. Using MAPS, the average lumen reduction of the resulting anastomoses was 57.98% with the maximum being 61.43%. However, research by Jahangiri et al. indicates that arteries can be reduced up to 70% while maintaining laminar flow [36]. Additional data from Dr. Mann et al. found a 5mm canine artery can be reduced by up to 90% before blood flow is reduced by 50% [37]. While studies seem to indicate lumen reduction of 57.98% might be acceptable, efforts should be applied to reduce this in future iterations. Tighter control of bite depth using OCT would help minimize lumen reduction.

In summary, MAPS successfully performed vascular anastomosis with minimal human intervention in 5 mm vessels. This size is applicable to femoral and brachial artery surgery [38], [39]. Enhancements to the system are needed to improve repeatability along with larger studies for validation, but in its current state MAPS offers better spacing variation when compared to previous STAR system studies. While 5 mm vessels were used in this study due to limitations with the size of STAR's needle driver, we envision that anastomosis of smaller vasculature, such as 1 mm vessels encountered in maxillofacial and head and neck reconstruction [40], [41] would be possible with a robotic needle driver that can support 9-0 suture. Notably, high resolution OCT imaging shows promise to make the system fully automatic and more accurate. While a human in the loop is necessary to run the system today, a feedback control loop where OCT data is used to inform correct suture placement would enable a fully autonomous system in future studies with the MAPS system.

VI. ACKNOWLEDGMENT

We would like to thank Lydia Zoghbi for her assistance in performing the tensile force testing presented in this work. We would also like to thank Dr. Iulian Iordachita for consultation in microvascular robotic techniques and technology.

REFERENCES

[1] J. B. West, "Pulmonary microvascular pressure and pulmonary edema," *Chest*, vol. 74, no. 1, pp. 117–118, Jul. 1978, doi: 10.1378/chest.74.1.118.

[2] S. M. Levin, "Alexis Carrel's historic leap of faith," *J Vasc Surg*, vol. 61, no. 3, pp. 832–833, Mar. 2015, doi: 10.1016/j.jvs.2013.09.012.

[3] A. Carrel and C. C. Guthrie, "Anastomosis of blood vessels by the patching method and transplantation of the kidney. 1906 [classical article]," *Yale J Biol Med*, vol. 74, no. 4, pp. 243–247, Aug. 2001.

[4] W. R. Moritz, S. Raman, S. Pessin, C. Martin, X. Li, A. Westman, and J. M. Sacks, "The History and Innovations of Blood Vessel Anastomosis," *Bioengineering (Basel)*, vol. 9, no. 2, p. 75, Feb. 2022, doi: 10.3390/bioengineering9020075.

[5] J. D. MacDonald, "Learning to Perform Microvascular Anastomosis," *Skull Base*, vol. 15, no. 3, pp. 229–240, Aug. 2005, doi: 10.1055/s-2005-872598.

[6] E. I. Chang, M. G. Galvez, J. P. Glotzbach, C. D. Hamou, S. El-ftesi, C. T. Rappleye, K.-M. Sommer, J. Rajadas, O. J. Abilez, G. G. Fuller, M. T. Longaker, and G. C. Gurtner, "Vascular anastomosis using controlled phase transitions in poloxamer gels," *Nat Med*, vol. 17, no. 9, pp. 1147–1152, Aug. 2011, doi: 10.1038/nm.2424.

[7] L. E. Chen, A. V. Seaber, and J. R. Urbaniak, "Microvascular anastomoses in growing vessels: a long-term evaluation of nonabsorbable suture materials," *J Reconstr Microsurg*, vol. 9, no. 3, pp. 183–189, May 1993, doi: 10.1055/s-2007-1006643.

[8] G. Kochhar, J. M. Parungao, I. A. Hanouneh, and M. A. Parsi, "Biliary complications following liver transplantation," *World J Gastroenterol*, vol. 19, no. 19, pp. 2841–2846, May 2013, doi: 10.3748/wjg.v19.i19.2841.

[9] N. Bonaros, T. Schachner, D. Wiedemann, A. Oehlinger, E. Ruetzler, G. Feuchtner, C. Kolbitsch, C. Velik-Salchner, G. Friedrich, O. Pachinger, G. Laufer, and J. Bonatti, "Quality of life improvement after robotically assisted coronary artery bypass grafting," *Cardiology*, vol. 114, no. 1, pp. 59–66, 2009, doi: 10.1159/000212115.

[10] N. Saegusa, S. Sarukawa, K. Ohta, K. Takamatsu, M. Watanabe, T. Sugino, M. Nakagawa, Y. Akiyama, M. Kusuhara, K. Kishi, and K. Inoue, "Sutureless microvascular anastomosis assisted by an expandable shape-memory alloy stent," *PLoS One*, vol. 12, no. 7, p. e0181520, Jul. 2017, doi: 10.1371/journal.pone.0181520.

[11] J. Finkelstein, E. Eckersberger, H. Sadri, S. S. Taneja, H. Lepor, and B. Djavan, "Open Versus Laparoscopic Versus Robot-Assisted Laparoscopic Prostatectomy: The European and US Experience," *Rev Urol*, vol. 12, no. 1, pp. 35–43, 2010.

[12] C. M. Kang, H. S. Chi, J. Y. Kim, G. H. Choi, K. S. Kim, J. S. Choi, W. J. Lee, and B. R. Kim, "A case of robot-assisted excision of choledochal cyst, hepaticojejunostomy, and extracorporeal Roux-en-y anastomosis using the da Vinci surgical system," *Surg Laparosc Endosc Percutan Tech*, vol. 17, no. 6, pp. 538–541, Dec. 2007, doi: 10.1097/SLE.0b013e318150e57a.

[13] C.-S. Lai, C.-T. Lu, S.-A. Liu, Y.-C. Tsai, Y.-W. Chen, and I.-C. Chen, "Robot-assisted microvascular anastomosis in head and neck free flap reconstruction: Preliminary experiences and results," *Microsurgery*, vol. 39, no. 8, pp. 715–720, Nov. 2019, doi: 10.1002/micr.30458.

[14] A. Shademan, R. S. Decker, J. D. Opfermann, S. Leonard, A. Krieger, and P. C. W. Kim, "Supervised autonomous robotic soft tissue surgery," *Sci. Transl. Med.*, vol. 8, no. 337, May 2016, doi: 10.1126/scitranslmed.aad9398.

[15] H. Saeidi, J. D. Opfermann, M. Kam, S. Wei, S. Leonard, M. H. Hsieh, J. U. Kang, and A. Krieger, "Autonomous robotic laparoscopic surgery for intestinal anastomosis," *Science Robotics*, vol. 7, no. 62, p. eabj2908, Jan. 2022, doi: 10.1126/scirobotics.abj2908.

[16] K. E. Matschke, J. F. Gummert, S. Demertzis, U. Kappert, M. B. Anssar, F. Siclari, V. Falk, E. L. Alderman, C. Detter, H. Reichenspurner, and W. Harringer, "The Cardica C-Port System: Clinical and angiographic evaluation of a new device for automated, compliant distal anastomoses in coronary artery bypass grafting surgery—A multicenter prospective clinical trial," *The Journal of Thoracic and Cardiovascular Surgery*, vol. 130, no. 6, pp. 1645–1652, Dec. 2005, doi: 10.1016/j.jtcvs.2005.08.033.

[17] M. J. Connor, P. Dasgupta, H. U. Ahmed, and A. Raza, "Autonomous surgery in the era of robotic urology: friend or foe of the future surgeon?," *Nature Reviews Urology*, vol. 17, no. 11, pp. 643–649, 2020.

[18] P. Heidekrueger, U. von Fritschen, N. Moellhoff, G. Germann, R. Giunta, F. Zeman, and L. Prantl, "Comparison of venous couplers versus hand-sewn technique in 4577 cases of DIEP-flap breast reconstructions – A multicenter study," *Microsurgery*, vol. 42, no. 1, pp. 5–12, 2022, doi: 10.1002/micr.30686.

[19] E. V. Barker and D. J. Enepekides, "The utility of microvascular anastomotic devices in head and neck reconstruction," *Current Opinion in Otolaryngology & Head and Neck Surgery*, vol. 16, no. 4, p. 331, Aug. 2008, doi: 10.1097/MOO.0b013e32830139a7.

[20] J. A. Spector, L. B. Draper, J. P. Levine, and C. Y. Ahn, "Routine Use of Microvascular Coupling Device for Arterial Anastomosis in Breast Reconstruction," *Annals of Plastic Surgery*, vol. 56, no. 4, p. 365, Apr. 2006, doi: 10.1097/01.sap.0000202614.45743.34.

[21] W. Jeong, K. Kim, D. Son, and Y. Kim, "New Absorbable Microvascular Anastomotic Devices Representing a Modified Sleeve Technique: Evaluation of Two Types of Source Material and Design," *Sci Rep*, vol. 9, no. 1, Art. no. 1, Jul. 2019, doi: 10.1038/s41598-019-47499-5.

[22] A. R. Gundale, Y. J. Berkovic, P. Entezami, C. O. Nathan, and B. A. Chang, "Systematic review of microvascular coupling devices for arterial anastomoses in free tissue transfer," *Laryngoscope Investig*

Otolaryngol, vol. 5, no. 4, pp. 683–688, Jul. 2020, doi: 10.1002/lio2.427.

[23] R. C. Harwell and R. L. Ferguson, "Physiologic tremor and microsurgery," *Microsurgery*, vol. 4, no. 3, pp. 187–192, 1983, doi: 10.1002/micr.1920040310.

[24] R. D. Katz, G. D. Rosson, J. A. Taylor, and N. K. Singh, "Robotics in microsurgery: use of a surgical robot to perform a free flap in a pig," *Microsurgery*, vol. 25, no. 7, pp. 566–569, 2005, doi: 10.1002/micr.20160.

[25] C. Taleb, E. Nectoux, and P. A. Liverneaux, "Telemicrosurgery: a feasibility study in a rat model," *Chir Main*, vol. 27, no. 2–3, pp. 104–108, Jun. 2008, doi: 10.1016/j.main.2008.04.001.

[26] R. Cau, "Design and realization of a master-slave system for reconstructive microsurgery," Phd Thesis 1 (Research TU/e / Graduation TU/e), Technische Universiteit Eindhoven, Eindhoven, 2014. doi: 10.6100/IR763107.

[27] T. J. M. van Mulken, C. A. E. M. Boymans, R. M. Schols, R. Cau, F. B. F. Schoenmakers, L. T. Hoekstra, S. S. Qiu, J. C. Selber, and R. R. W. J. van der Hulst, "Preclinical Experience Using a New Robotic System Created for Microsurgery," *Plast Reconstr Surg*, vol. 142, no. 5, pp. 1367–1376, Nov. 2018, doi: 10.1097/PRS.0000000000004939.

[28] M. Mitsuishi, A. Morita, N. Sugita, S. Sora, R. Mochizuki, K. Tanimoto, Y. M. Baek, H. Takahashi, and K. Harada, "Master-slave robotic platform and its feasibility study for micro-neurosurgery," *Int J Med Robot*, vol. 9, no. 2, pp. 180–189, Jun. 2013, doi: 10.1002/rcs.1434.

[29] C. D'Ettorre, G. Dwyer, X. Du, F. Chadebecq, F. Vasconcelos, E. De Momi, and D. Stoyanov, "Automated Pick-Up of Suturing Needles for Robotic Surgical Assistance," in *2018 IEEE International Conference on Robotics and Automation (ICRA)*, May 2018, pp. 1370–1377. doi: 10.1109/ICRA.2018.8461200.

[30] S. A. Pedram, P. Ferguson, J. Ma, E. Dutson, and J. Rosen, "Autonomous suturing via surgical robot: An algorithm for optimal selection of needle diameter, shape, and path," in *2017 IEEE International Conference on Robotics and Automation (ICRA)*, May 2017, pp. 2391–2398. doi: 10.1109/ICRA.2017.7989278.

[31] S. Sen, A. Garg, D. V. Gealy, S. McKinley, Y. Jen, and K. Goldberg, "Automating multi-throw multilateral surgical suturing with a mechanical needle guide and sequential convex optimization," in *2016 IEEE International Conference on Robotics and Automation (ICRA)*, May 2016, pp. 4178–4185. doi: 10.1109/ICRA.2016.7487611.

[32] B. F. de Menezes, F. V. de Oliveira, M. S. Secanho, L. B. Carvalho, W. R. Moragas, and M. S. Fernandes, "Submerged vascular anastomosis. A technique for vascular suturing in experimental microsurgery," *Acta Cir Bras*, vol. 36, no. 8, p. e360807, doi: 10.1590/ACB360807.

[33] C. A. Schneider, W. S. Rasband, and K. W. Eliceiri, "NIH Image to ImageJ: 25 years of image analysis," *Nat Methods*, vol. 9, no. 7, Art. no. 7, Jul. 2012, doi: 10.1038/nmeth.2089.

[34] J. Forkman, "Estimator and Tests for Common Coefficients of Variation in Normal Distributions," *Communications in Statistics - Theory and Methods*, vol. 38, no. 2, pp. 233–251, Jan. 2009, doi: 10.1080/03610920802187448.

[35] M. Heitzer, J. Brockhaus, K. Kniha, F. Merkord, F. Peters, F. Hölzle, E. Goloborodko, and A. Modabber, "Mechanical strength and hydrostatic testing of VIVO adhesive in sutureless microsurgical anastomoses: an ex vivo study," *Sci Rep*, vol. 11, no. 1, Art. no. 1, Jun. 2021, doi: 10.1038/s41598-021-92998-z.

[36] M. Jahangiri, M. Saghafian, and M. R. Sadeghi, "Numerical Study of Turbulent Pulsatile Blood Flow through Stenosed Artery Using Fluid-Solid Interaction," *Computational and Mathematical Methods in Medicine*, vol. 2015, pp. 1–10, 2015, doi: 10.1155/2015/515613.

[37] F. C. Mann, J. F. Herrick, H. E. Essex, and E. J. Baldes, "The effect on the blood flow of decreasing the lumen of a blood vessel," *Surgery*, vol. 4, no. 2, pp. 249–252, Aug. 1938, doi: 10.5555/uri:pii:S0039606038902946.

[38] K. S. Spector and W. E. Lawson, "Optimizing safe femoral access during cardiac catheterization," *Catheter Cardiovasc Interv*, vol. 53, no. 2, pp. 209–212, Jun. 2001, doi: 10.1002/ccd.1150.

[39] G. F. Mitchell, H. Parise, J. A. Vita, M. G. Larson, E. Warner, J. F. Keaney, M. J. Keyes, D. Levy, R. S. Vasan, and E. J. Benjamin, "Local Shear Stress and Brachial Artery Flow-Mediated Dilation," *Hypertension*, vol. 44, no. 2, pp. 134–139, Aug. 2004, doi: 10.1161/01.HYP.0000137305.77635.68.

[40] S. K. Mudigonda, S. Murugan, K. Velavan, S. Thulasiraman, and V. B. Krishna Kumar Raja, "Non-suturing microvascular anastomosis in maxillofacial reconstruction- a comparative study," *J Craniomaxillofac Surg*, vol. 48, no. 6, pp. 599–606, Jun. 2020, doi: 10.1016/j.jcms.2020.04.005.

[41] M. D. DeLacure, R. S. Wong, B. L. Markowitz, M. R. Kobayashi, C. Y. Ahn, D. P. Shedd, A. L. Spies, T. R. Loree, and W. W. Shaw, "Clinical experience with a microvascular anastomotic device in head and neck reconstruction," *Am J Surg*, vol. 170, no. 5, pp. 521–523, Nov. 1995, doi: 10.1016/s0002-9610(99)80344-4.